

Characterization of active sites on Rh/SiO₂ model catalysts

Sean M McClure, M Lundwall, F Yang, Z Zhou and D W Goodman¹

Department of Chemistry, Texas A&M University, PO Box 30012, College Station, TX 77842-3012, USA

E-mail: goodman@mail.chem.tamu.edu

Received 19 May 2009

Published 5 November 2009

Online at stacks.iop.org/JPhysCM/21/474223

Abstract

Rh/SiO₂ model catalyst surfaces are prepared under ultra-high vacuum conditions and examined *in situ* using scanning tunneling microscope and CO infrared reflection absorption techniques, to quantify the number and kinds of active Rh surface sites available for kinetic reaction (CO oxidation) as a function of Rh particle size. The results are compared against CO desorption measurements and elevated pressure CO oxidation reaction kinetics, to evaluate the extent of the correlation between the low and elevated pressure site characterization techniques. Data demonstrate that estimates of Rh active sites exhibit good agreement between the characterization methods and illustrate the utility of low pressure surface science characterization techniques in understanding elevated pressure reaction kinetics on model catalyst surfaces.

(Some figures in this article are in colour only in the electronic version)

1. Introduction

Oxide supported metal nanoparticles comprise the active phase of many heterogeneous catalysts. Fundamental studies of technical catalyst surfaces on a molecular level can be difficult due to the complicated nature of the catalyst surface (porosity, residual synthesis materials, etc). This poses a challenge for the study of catalytic reactions, as the selectivity and activity of many reactions exhibit a dependence on particle size (e.g. CO oxidation on Au particles [1]) and/or exposed surface structure (e.g. C₂H₆ hydrogenolysis on Ni surfaces [2]). In such reaction systems, accurate surface characterization becomes critical to understanding and designing more selective and active catalysts. To overcome the difficulties in characterizing the active surface of technical catalysts, 'model' catalyst surfaces, consisting of well-defined particles on a planar oxide support, have been successfully employed to study the properties and behavior of catalytically active particles [3–8]. Often, such surfaces are generated via various deposition techniques in ultra-high vacuum (UHV) environments [9–22] where low pressure analytical techniques (STM, temperature programmed desorption (TPD), Auger electron spectroscopy (AES)) can be employed to study the surface. When coupled

with a contiguous high pressure reactor, kinetic reactivity measurements can be conducted on these surfaces under pressures approaching those more typical of working catalysts (approaching 1 atm). Bridging the divide between these pressure regimes has been a challenge for researchers, as elevated pressure conditions can modify the active surface in certain systems [23]. Understanding the extent of correlation between characterization studies conducted via low pressure and elevated pressure techniques is an important part of bridging the pressure gap.

To gain further insight into this issue, we have performed studies characterizing Rh/SiO₂ model catalyst surfaces under both low and elevated pressure environments. Three different techniques, conducted under low pressure (STM, CO TPD) and elevated pressure (CO₂ oxidation kinetics) conditions, are employed to estimate Rh active sites (sites cm⁻²) as a function of Rh coverage. CO infrared reflection absorption (CO-IRAS) spectroscopy is employed to probe particle morphology as a function of particle size. Active site estimates from the three techniques are compared and demonstrate general agreement between the three methods of site characterization. These results illustrate that characterization of model catalyst surfaces conducted under low pressure conditions can provide useful insights into the nature of catalytically active particle surfaces under elevated pressures.

¹ Author to whom any correspondence should be addressed.

2. Experimental details

Experiments were conducted in a coupled high pressure reactor–UHV surface analysis chamber described previously, which allows for *in situ* translation of surfaces prepared in the UHV chamber into the reactor cell [24, 25]. A Rh(111) sample (circular disk, 0.963 cm diameter) was used for single crystal reactivity, TPD and IRAS measurements. A Mo(112) single crystal sample (circular disk, 0.986 cm diameter) was used as a substrate for Rh/SiO₂ model catalyst growth. Model catalyst surfaces were generated using vapor deposition techniques discussed previously [25–27] in two steps: (1) preparation of SiO₂ film on the Mo(112) substrate and (2) vapor deposition of Rh metal on the SiO₂ film at $T = 300$ K. SiO₂ films for reactivity studies were approximately 5 ML thick, as determined by attenuation of the Mo(187 eV) AES feature. Rh coverages are reported in monolayer (ML), as determined from AES breakpoint analysis of Rh deposited on Mo(112); Rh(302 eV)/Mo(187 eV) AES ratio = 0.5 corresponds to 1.0 ML Rh [25]. Elevated pressure CO oxidation reactions were conducted in a batch reactor mode using a baratron gauge method described previously [28]. Ultra-high purity (UHP) CO was further purified via molecular sieve and LN₂ trapping; UHP O₂ was used without further purification.

CO-IRAS measurements were conducted with a Mattson Cygnus 100 infrared spectrometer. The model catalyst surfaces were prepared and translated *in situ* to the contiguous IR/reaction cell, which is equipped with CaF₂ windows. Prior to CO-IRAS measurements, Rh/SiO₂ surfaces were cleaned with O₂ (5×10^{-6} Torr, 600 K, 10 min). The IR beam impinged the sample through the CaF₂ windows with an incident angle of 85° with respect to the surface normal. IR spectra were typically collected using 512 scans (spectra resolution 4 cm⁻¹) with a liquid nitrogen-cooled mercury cadmium telluride (MCT) detector. Absorbance is calculated with respect to a reference spectra taken of the clean Rh/SiO₂ sample at $T = 300$ K.

STM measurements were conducted in a separate vacuum system. Rh particles were deposited on an ultra-thin (1 ML SiO₂) film at $T = 300$ K under UHV conditions. The ultra-thin silica film was prepared by the oxidization of deposited Si atoms on Mo(112) and subsequent annealing to remove multi-layer SiO₂. Prior to Si deposition, the sample was flashed to 2100 K and then oxidized in 5×10^{-8} Torr O₂ at 850 K for 7 min. A p(2 × 3)-O surface was obtained after the oxidation. The silica film was then prepared by depositing less than 1 ML Si onto a Mo(112)-p(2 × 3)-O surface, followed by annealing at 800 K in 5×10^{-8} Torr O₂ for 5 min then increasing the temperature to 1200 K for an additional 10 min. This Si deposition/oxidation/annealing procedure was repeated several times until a constant Si/Mo AES ratio was achieved. The silica film was then annealed in UHV at 1200 K for 5 min. Rh coverages were calibrated via AES breakpoint analysis, and exhibited results identical to samples used for reactivity measurements.

3. Results and discussion

3.1. STM measurements of Rh/SiO₂ particles

Shown in figures 1(a)–(c) are representative particle histograms (particle count versus d_p (nm)) for 0.5, 1.0 ML, and

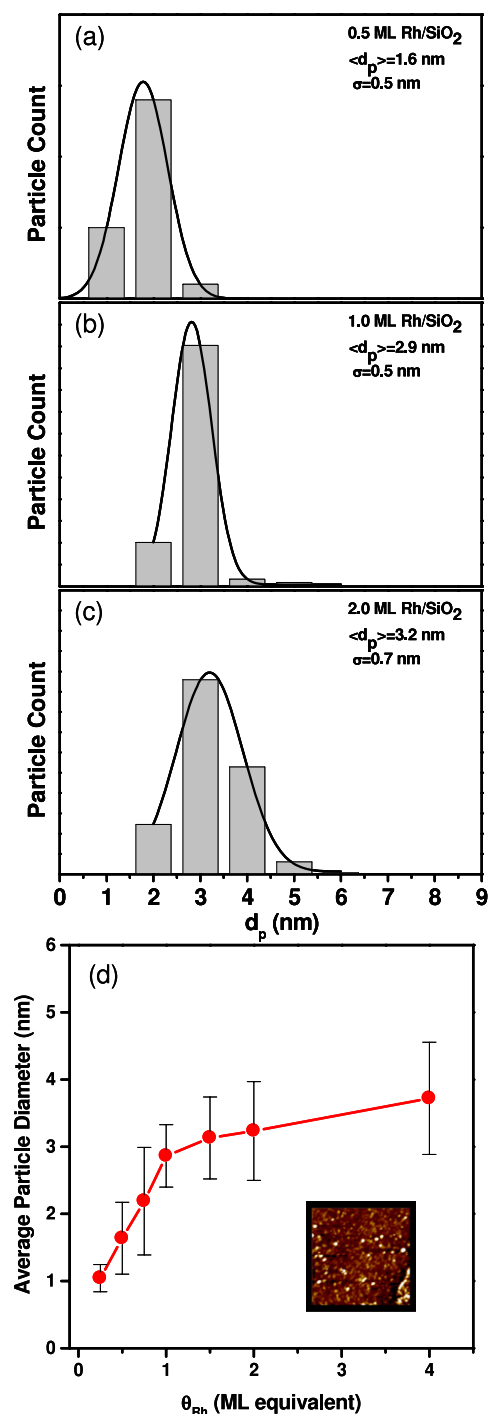


Figure 1. (a)–(c) Particle histogram data (particle count versus d_p (nm)) for 0.5, 1.0 ML, and 2.0 ML Rh/SiO₂ surfaces, respectively. Average particle diameter ($\langle d_p \rangle$) and standard deviation of the distribution (σ) are reported for each coverage. Inset: Representative STM image of the 0.5 ML Rh/SiO₂ surface (image size: 50 nm × 50 nm). (d) Average particle diameter (nm) versus θ_{Rh} (ML) obtained from histogram data for 0.25–4.0 ML Rh/SiO₂ samples. Error bars represent standard deviation ($\pm\sigma$) as determined from particle histogram data at each θ_{Rh} .

2.0 ML model catalyst surfaces. Shown in the inset of 1(d) is a representative STM images for the 0.5 ML Rh/SiO₂ surface. Histogram data can be analyzed to determine the average

particle size ($\langle d_p \rangle$) and standard deviation (σ) for the as-prepared samples. Shown in figure 1(d) is the average Rh particle diameter (nm) versus θ_{Rh} , obtained from particle histograms collected from STM images of Rh/SiO₂ samples of varying Rh coverage (θ_{Rh}), over the $\theta_{\text{Rh}} = 0.25\text{--}4.0$ ML coverage range. As the data illustrate, mean particle size of the Rh particles (bright spots in the image) and σ increase as a function of Rh coverage. The largest change in particle size occurs between 0.25 and 1.0 ML θ_{Rh} coverages, which corresponds to a change from 1.0 to 2.9 nm diameter particles, respectively. Particle heights measured from the Rh/SiO₂ surfaces indicate an aspect ratio (h/d_p) of approximately 0.4, consistent for particles of all sizes, and suggest Rh particles form a pseudo-hemispherical shape at the silica film surface. As further characterization data and analyses will demonstrate, figure 1(d) can provide a relation between average particle size and θ_{Rh} of model surfaces used for elevated pressure kinetic studies.

3.2. CO-IRAS of Rh/SiO₂ and Rh(111) surfaces

Infrared spectra of CO adsorption on Pt-group metals can offer insights into the nature of particle morphology and available CO binding sites on the Rh/SiO₂ surfaces. CO stretching frequencies ($\nu_{\text{CO}}(\text{cm}^{-1})$) exhibit shifts based on CO binding environment (e.g. atop, bridging, three-fold hollow) [29]. Shown in figure 2(a) inset is a CO-IRAS spectra obtained from a CO saturated Rh(111) surface at $T = 300$ K, for reference comparison to the Rh/SiO₂ samples. In accord with previous detailed IRAS and HREELS studies of the CO/Rh(111) system, CO adsorbs in atop positions (feature at $\nu_{\text{CO}} = 2064 \text{ cm}^{-1}$) and three-fold hollow positions (feature at $\nu_{\text{CO}} = 1865 \text{ cm}^{-1}$) at saturation coverages [30–33]. As temperature is increased (data not shown for Rh(111)), the CO coverage is decreased, resulting in the disappearance of the three-fold hollow feature followed by dipole induced peak shifts to lower wavenumbers of the atop CO feature. Shown in figures 2(a) and (b) are representative temperature dependent CO-IRAS spectra obtained from $\langle d_p \rangle = 2.9$ nm ($\theta_{\text{Rh}} = 1.0$ ML) and $\langle d_p \rangle = 3.7$ nm ($\theta_{\text{Rh}} = 4.0$ ML) Rh/SiO₂ surfaces. CO spectra are obtained at $\Delta T = 25$ K increments in an environment of $P = 5 \times 10^{-7}$ Torr CO, starting from an initial temperature of $T = 300$ K. At saturation coverages, CO exhibits an atop adsorption feature at $\nu_{\text{CO}} = 2070\text{--}2075 \text{ cm}^{-1}$ on both the 2.9 and 3.7 nm Rh/SiO₂ surfaces. A less intense, broad adsorption feature is observed between 1875 and 1975 cm^{-1} for the 3.7 nm (4.0 ML) surface at $T = 300$ K; as will be discussed shortly, this feature is similar to a bridging bound (2- or 3-fold coordinated) CO binding feature which has been observed on previous studies of Rh/Al₂O₃ [9, 10] and Rh/TiO₂ model catalysts [34]. As the temperature is increased, CO-IRAS spectra exhibit trends in agreement with previous observations of CO on Rh surfaces. With increasing T , the CO surface coverage is decreased due to an increase in the CO desorption rate, as evidenced by the concomitant (1) decrease in IRAS signal intensity and (2) peak shift to lower wavenumbers. This shift to lower wavenumbers is consistent with decreased dipole coupling of the CO molecules as CO coverage is decreased. Surface concentration of CO is below

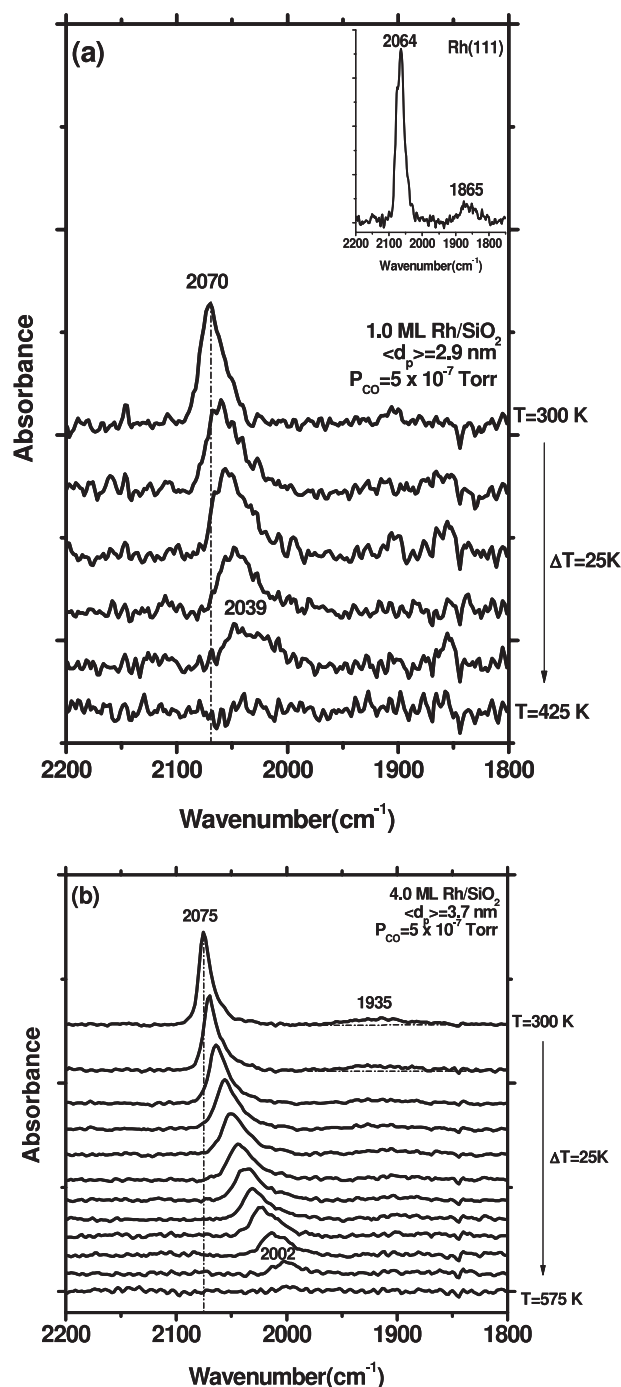


Figure 2. (a) Temperature dependent CO-IRAS spectra obtained for CO adsorption on a $\langle d_p \rangle = 2.9$ nm (1.0 ML) Rh/SiO₂ surface. Initial temperature $T = 300$ K, T is increased in $\Delta T = 25$ K increments for IR spectra collection. Inset: CO-IRAS spectra of saturation CO coverage on Rh(111) single crystal at $T = 300$ K. (b) Temperature dependent CO-IRAS spectra obtained for CO adsorption on a $\langle d_p \rangle = 3.7$ nm (4.0 ML) Rh/SiO₂ surface. Initial temperature $T = 300$ K, T is increased in $\Delta T = 25$ K increments for IR spectra collection.

detection limit above temperatures of $T = 550$ K for all the surfaces studied. Similar temperature dependent CO-IRAS behavior was observed for all coverages studied (0.5–10 ML).

Figure 3 shows CO-IRAS spectra obtained in $P_{\text{CO}} = 5 \times 10^{-7}$ at room temperature, $T = 300$ K, for various

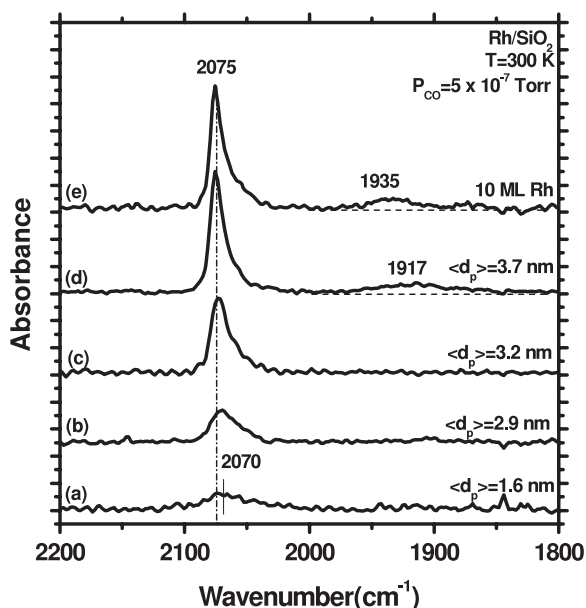


Figure 3. (a)–(e) θ_{Rh} dependent CO-IRAS spectra for coverages (a) 0.5 ML, (b) 1.0 ML, (c) 2.0 ML, (d) 4.0 ML, (e) 10 ML Rh. All spectra obtained in $P_{\text{CO}} = 5 \times 10^{-7}$ Torr, $T = 300$ K. Average particle sizes for coverages $\langle d_p \rangle$ denoted in spectra.

θ_{Rh} coverages (0.5–10 ML). As one would expect, CO-IRAS intensity increases as Rh coverage is increased. A slight shift (2070–2075 cm^{-1}) in ν_{CO} to higher wavenumbers is observed as the coverage (and particle size) is increased. This slight shift could be due to increased dipole–dipole coupling between surface bound CO molecules, which may be more pronounced on larger particles which could accommodate more CO (larger close packed (111), (100) facets). As the Rh particle size is increased (to 4.0 ML and above), the second, broad ν_{CO} feature observed at lower wavenumbers becomes visible in the CO-IRAS spectra; this ν_{CO} is consistent with a bridging bound CO surface species observed in previous CO-IRAS studies of Rh/ Al_2O_3 surfaces [9, 10]. This bridging type feature is less pronounced on the Rh/ SiO_2 surface prepared with lower Rh coverages, presumably due to the lower amount of adsorbed CO present on the surface, which attenuates the intensity of the CO-IRAS features.

Detailed work by Freund and co-workers has examined CO adsorption employing CO-IRAS on Rh/ Al_2O_3 model catalyst surfaces [9, 10]. Infrared spectra obtained by these investigators on samples grown or annealed to $T > 300$ K, also show atop (2080 cm^{-1}) and bridging (1770–1950 cm^{-1}) bound CO features, similar to those observed in the present study. Similarly, infrared studies of CO adsorption on technical catalysts also show characteristic atop and bridging features consistent with those observed in the present study [35, 36]. Features associated with Rh gem dicarbonyl $\text{Rh}(\text{CO})_2$ species ($\nu_{\text{CO,sym}} \sim 2090\text{--}2110$ cm^{-1} , $\nu_{\text{CO,asym}} \sim 2020\text{--}2035$ cm^{-1}) were not observed over the particle size ranges employed in this study. These additional CO stretching features have been observed in previous studies of highly dispersed, low temperature prepared Rh/ Al_2O_3 model catalyst surfaces [9, 10] and infrared studies of CO adsorption on technical catalysts

surfaces under elevated pressure conditions [35, 36]. Though found to be a rather inactive species for CO oxidation under elevated pressure conditions (compared to atop-bridging bound CO) [37–39], the absence of these features in the CO-IRAS spectra allows additional insights into the nature of our particle surfaces. Coupled STM and CO-IRAS studies of Rh/ Al_2O_3 model catalyst surfaces by Freund and co-workers [9, 10], prepared at low temperatures ($T \sim 90$ K) with sub-monolayer Rh coverages, exhibit a gem dicarbonyl stretching feature near $\nu_{\text{CO}} = 2117$ cm^{-1} , due to atomically dispersed $\text{Rh}(\text{CO})_2$ species present at oxide defects. If Rh is deposited at $T = 300$ K, Rh atoms have sufficient surface mobility to form larger particles, eliminating the concentration of highly dispersed Rh species [9, 10]. A similar picture has been observed in CO infrared studies of Rh/ $\text{TiO}_2(110)$ model catalyst surfaces, which demonstrate high temperature treatments of Rh particles can eliminate dicarbonyl stretching features [34]. Infrared CO adsorption studies on bulk catalyst surfaces are qualitatively consistent with these observations [35, 36]. A survey study by Trautmann *et al* of Rh clusters supported on various oxides (SiO_2 , Al_2O_3 , TiO_2) demonstrate gem dicarbonyl CO features present in IR spectra. These stretching frequencies are essentially constant with increasing coverage (indicative of isolated sites) and tend to attenuate with increasing temperature, observations consistent with stretching features associated with isolated $\text{Rh}(\text{CO})_2$ -type species [35]. Studies by Cavanagh *et al* have also demonstrated via infrared studies of alumina supported Rh particles, that the presence of spatially isolated $\text{Rh}(\text{CO})_2$ dicarbonyl species is prevalent on highly dispersed samples, which exhibit the characteristic gem dicarbonyl stretching frequencies near $\nu_{\text{CO}} = 2101$ and 2030 cm^{-1} [36]. It is likely the case that our surfaces contain Rh particle sizes too large and have been prepared at temperatures too high ($T = 300$ K) to produce a detectable concentration of dicarbonyl surface species, as these species appear to be associated with atomically dispersed Rh. This also suggests that CO induced disruption of our Rh particles (breakup of particles to form $\text{Rh}(\text{CO})_2$) [19] is not detectable via CO-IRAS for the particle sizes employed, under the experimental conditions of the infrared studies. To summarize, low pressure CO-IRAS studies of Rh/ SiO_2 catalyst surfaces, prepared at $T = 300$ K across the ($\langle d_p \rangle = 1\text{--}4$ nm) range, exhibit CO species characteristic of atop bound ($\nu_{\text{CO}} = 2070\text{--}2075$ cm^{-1} , at saturation $T = 300$ K) and bridging bound ($\nu_{\text{CO}} = 1875\text{--}1975$ cm^{-1}) CO surface species, as observed previously in the literature.

3.3. Comparison of reactivity, chemisorption and STM active site estimates

CO oxidation on Pt-group metal single crystal surfaces under elevated pressure conditions is a well studied, benchmark reaction system. Numerous investigations have demonstrated that under elevated pressure conditions (pressures approaching 1 atm and CO-rich reaction conditions) and relevant catalytic temperatures ($T = 450\text{--}625$ K), the CO oxidation reaction on Rh exhibits structure insensitive behavior; i.e. observed catalytic activity does not depend upon the underlying crystal

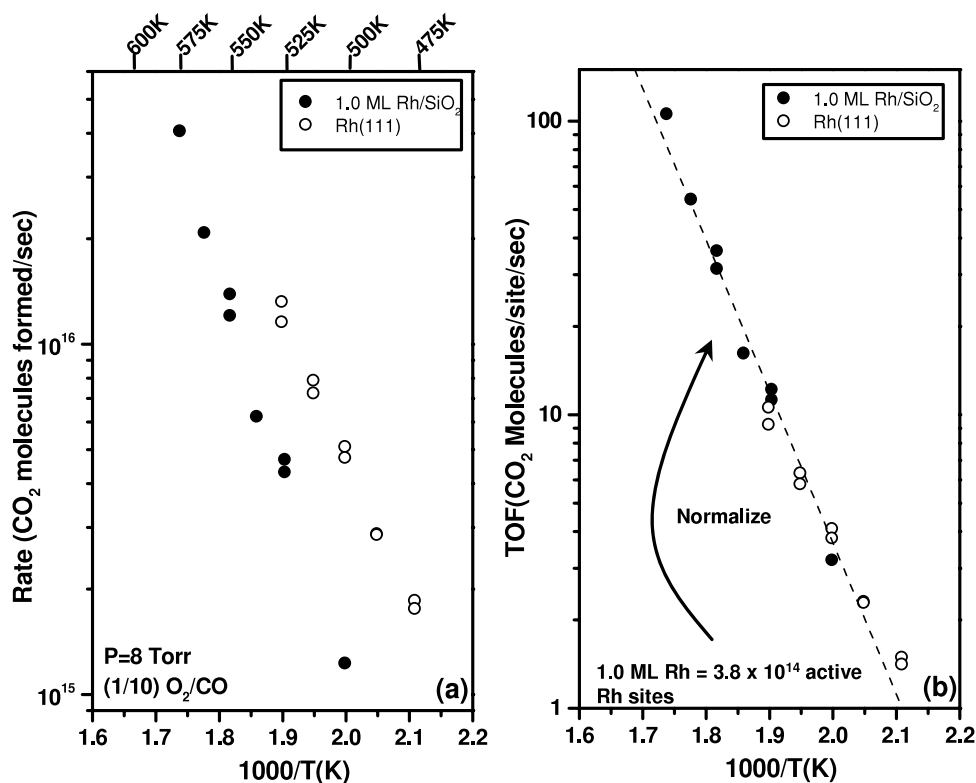


Figure 4. (a) CO₂ reaction rate data ((CO₂ molecules formed s⁻¹) versus 1000/*T* (K)) for a 1.0 ML Rh/SiO₂ (●) and Rh(111) (○) sample (rate corresponding to one side of the Rh(111) sample). *P* = 8.0 Torr; (1/10) O₂/CO gas mixture ratio. (b) CO₂ turnover frequency (TOF) (CO₂ molecules formed/site sec) versus 1000/*T* (K)) for a 1.0 ML Rh/SiO₂ (●) and Rh(111) (○) sample, as determined by normalization of Rh/SiO₂ data. *P* = 8.0 Torr; (1/10) O₂/CO gas mixture ratio.

structure [40–44]. This view has been further validated by the good agreement of single crystal data with high surface area supported catalyst data [40–44]. Technical catalyst studies employing different size Rh particles in the CO-inhibited regime, have also verified this structure insensitive behavior (<1–70 nm particles) [45]. Under such conditions, CO₂ formation is rate limited by the CO desorption step, as CO blocks sites for O₂ adsorption and dissociation. This view agrees with the observed positive order dependence on O₂ pressure, negative order dependence on CO pressure, and the similarity of the observed reaction activation energy with the CO desorption activation energy [46]. Under sufficiently O₂ rich reaction conditions and elevated temperatures (under UHV conditions [12, 47, 48] or under elevated pressures [40, 41, 49]), reactivity behavior can begin to exhibit structure sensitivities; these reaction conditions are not probed in the present study.

Due to the structure insensitivity of the CO oxidation reaction under CO-rich reaction conditions, carefully conducted elevated pressure measurements can provide a means for characterizing the active surface sites of model catalyst samples under elevated pressures, as the rate is proportional to the number of active Rh sites. Shown in figure 4 are reactivity measurements obtained on a 1.0 ML Rh/SiO₂ samples under highly CO-rich reaction conditions (O₂/CO = 1/10), *P* = 8.0 Torr, along with concurrent data obtained on the Rh(111) single crystal under identical conditions. Figure 4(a) shows the CO₂ production rate (CO₂ molecules produced s⁻¹) versus

1000/*T* (K). As the data illustrates, activation energy of CO oxidation on the Rh/SiO₂ surface and the Rh(111) single crystal surface are similar ($E \sim 110$ kJ mol⁻¹). By normalizing the reactivity data of the Rh/SiO₂ surface of figure 4(a) to the Rh(111) reactivity data, one can gain an estimate of the number of active sites present on the Rh/SiO₂ surface (figure 4(b)). For the case of the 1.0 ML Rh/SiO₂ surface, this corresponds to 3.8×10^{14} total active sites. By conducting this same exercise over a range of $\theta_{\text{Rh}} = (0.25\text{--}10$ ML), one can estimate the number of active sites as a function of θ_{Rh} under elevated pressure conditions. The results of these calculations, in terms of active Rh sites cm⁻², are displayed in figure 5. As expected, Rh sites cm⁻² increases as θ_{Rh} increases, approaching a concentration near the Rh(111) surface atom density at high θ_{Rh} .

CO thermal desorption measurements can provide a second method for active site characterization of Rh/SiO₂ samples [25]. Rh/SiO₂ samples are prepared with various coverages ($\theta_{\text{Rh}} = 1.0, 2.0, 4.0$ and 10 ML), and saturation doses of CO are delivered to the sample at low temperature (*T* = 175 K, *P*_{CO} = 4 L (1 Langmuir = 10⁻⁶ Torr s)). CO saturated surfaces are heated (ramp rate, $\beta \sim 5$ K s⁻¹) and CO desorption is monitored via a quadrupole mass spectrometer (*m/z* = 28) to obtain a measure of CO molecules adsorbed to the Rh nanoparticle surfaces. By comparing integrated TPD spectra from Rh/SiO₂ surfaces to that from a saturation dose on the Rh(111) surface, one can obtain an estimate of Rh sites as a function of θ_{Rh} . TPD experiments

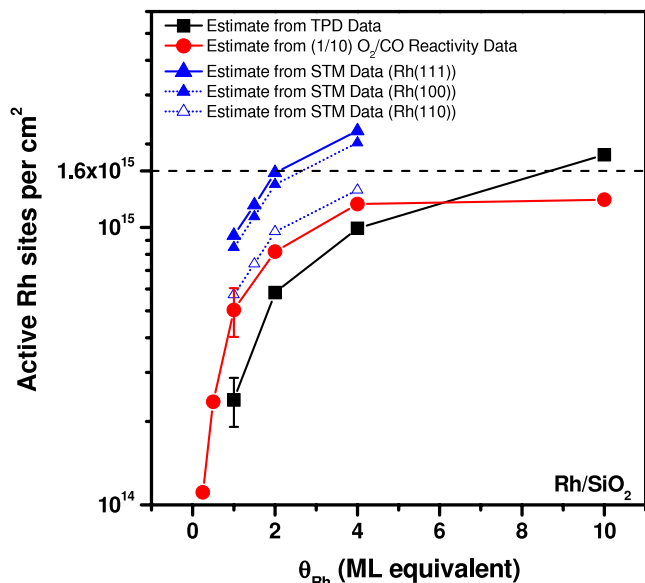


Figure 5. Estimates of active Rh sites cm^{-2} based on STM (\blacktriangle : (assuming Rh(111) surface atom density), $\text{---}\blacktriangle\text{---}$: (assuming Rh(100) surface atom density), \triangle : (assuming Rh(110) surface atom density)), CO TPD (\blacksquare), and elevated pressure reaction (\bullet) characterization techniques as a function of θ_{Rh} .

were conducted (spectra not shown here) for Rh/SiO₂ surfaces of $\theta_{\text{Rh}} = 1.0, 2.0, 4.0,$ and 10 ML , along with the Rh(111) for calibration. TPD spectra exhibited desorption behavior generally similar to that observed on Rh(111) and Rh model catalyst surfaces [30, 50, 51] (CO desorption in the $T = 300\text{--}500 \text{ K}$ range). These observations are also consistent with the CO-IRAS results of figures 2 and 3, which show undetectable CO surface coverages above $T = 550 \text{ K}$ in $P_{\text{CO}} = 2 \times 10^{-7} \text{ Torr}$ environment. Since the surface density of Rh(111) is $1.6 \times 10^{15} \text{ atoms cm}^{-2}$, these measurements can be employed to estimate the number of active Rh sites cm^{-2} , as shown in figure 5. As expected, Rh sites cm^{-2} increases with increasing θ_{Rh} . CO TPD spectra obtained from samples with $\theta_{\text{Rh}} < 1.0 \text{ ML}$ exhibited features which were too obscured by background CO desorption from the sample leads for accurate integrations. We estimate that the error in TPD measurements/integration is likely $\pm 20\%$ (error bars shown in figure 5), due to such background effects.

As a third method for active site estimation, STM histogram data (such as those displayed in figure 1) can be used to estimate the number of active Rh sites cm^{-2} as a function of θ_{Rh} , using a few simplifying geometric arguments. First, to remove the influence of tip apex in size measurement, we calibrated the measured particle diameter based on the Rh deposition rate. Assuming (1) the sticking probability of Rh on the thin silica film is 1 and (2) all Rh particles were exaggerated by the same factor, χ , due to the tip apex, we normalized the total calculated volume of Rh particles to the total deposition volume of Rh, by solving the equation, $\sum_{i=1}^n \frac{\pi h_i [3(r_i \chi)^2 + h_i^2]}{6} = V_{\text{dep}}$. The volume equation of a spherical cap, $\frac{\pi h [3r^2 + h^2]}{6}$, is then used here to calculate the volume of each Rh particle. V_{dep} is the amount of deposited Rh, calculated from the flux rate of Rh

times the deposition time (flux rate of Rh is $0.045 \text{ ML min}^{-1}$). Calculations for coverages of $\theta_{\text{Rh}} = 1.0, 1.5, 2.0,$ and 4.0 ML samples were used ($100 \text{ nm} \times 100 \text{ nm}$ images).

Based on the calibrated particle height and diameter (aspect ratio; $(h/d) \sim 0.4$ across particle sizes), a geometric estimate of the total surface sites of the UHV prepared sample can now be calculated based on the equation for the spherical cap surface, $A = 2\pi r h$ for the range of θ_{Rh} coverages above, assuming a surface atom density of $1.6 \times 10^{15} \text{ atoms cm}^{-2}$ (Rh(111) surface atom density). The result of this calculation is shown in figure 5. This assumption will likely provide an overestimate of the number of active Rh sites as particles approach smaller sizes and more corrugated surface facets. As such, we have calculated the active site density assuming less-densely packed facets for the Rh particles (Rh(100) = $1.45 \times 10^{15} \text{ atoms cm}^{-2}$ and Rh(110) = $9.8 \times 10^{14} \text{ atoms cm}^{-2}$), as shown in figure 5.

All three site estimation methods (CO TPD, CO₂ reactivity, and STM) have been plotted in figure 5, which displays Rh sites cm^{-2} as a function of θ_{Rh} . The data illustrates that general agreement is achieved between three methods, with methods tracking well with one another as a function of coverage. As expected, STM estimates using Rh(111) surface atom density slightly overestimates the number of active sites present on the Rh/SiO₂ surface. Estimates employing Rh(100) and Rh(110) surface atom densities (facets more characteristic of smaller particles) begin to approach the reactivity and TPD data to provide better agreement, though are still overall slightly higher. We speculate that this slight disagreement likely arises from the simplifying assumptions associated with the geometric STM estimation method. CO TPD and CO reactivity measurements show good agreement with one another.

Taken together, we interpret these results to indicate that the three characterization measurements employed provide consistent estimates of the number of Rh active sites as a function of θ_{Rh} . This is surprising, considering the $\sim 10^{10}$ order of magnitude difference in pressure range over which the characterization measurements were taken (STM, CO TPD measurements: $P = 10^{-10} \text{ Torr}$; CO oxidation reactivity measurements: $P = 8 \text{ Torr}$). The data suggest that, under the conditions of our study, particle sizes obtained via STM measurements appear to provide a reasonable estimate of the particle sizes characteristic of those present during elevated pressure reactivity measurements. As such, elevated pressure reactivity measurements conducted on Rh/SiO₂ surfaces, which are calibrated by Rh coverage, can be related to a measurement of average particle size $\langle d_p \rangle$ (figure 1(d)) as an approximation of particle size characteristic of reactivity measurements. These characterization studies will provide a useful benchmark for future studies of structure sensitive reactions on model catalyst surfaces at elevated pressures, reactions whose activity and selectivity are strongly dependent on particle size. Additionally, these results affirm the structure insensitivity of the CO oxidation reaction under CO-rich conditions and illustrate the utility of model catalyst surfaces in providing quantitative and qualitative reactivity data under elevated pressures.

4. Conclusions

We have performed studies characterizing Rh/SiO₂ model catalyst surfaces under both low and elevated pressure environments. Three different techniques under low pressure (STM, CO TPD) and elevated pressure (CO₂ oxidation kinetics) conditions were employed to estimate Rh active sites (sites cm⁻²) as a function of Rh coverage. CO infrared (IRAS) spectroscopy was employed to assess the CO binding characteristics of the Rh/SiO₂ surfaces. Our primary conclusions are summarized below.

- (1) Low pressure CO-IRAS measurements indicate atop and multiply coordinated CO binding sites across the particle size ranges (1–4 nm) examined. No CO-IRAS evidence for Rh gem dicarbonyl species was observed. Stretching frequencies are consistent with atop and bridging type CO binding sites observed in previous infrared studies of Rh surfaces.
- (2) Estimates of Rh active sites based on three characterization methods exhibit general agreement, despite the wide range of pressure conditions over which characterization measurements were conducted (10⁻¹⁰ Torr (UHV STM and TPD measurements) and 8 Torr (elevated pressure reactivity measurements)). The good agreement of the TPD and reactivity measurements, and the broad agreement of all three methods indicate that CO oxidation measurements, run under CO-rich conditions, can provide a reasonable estimate of the number of active sites present on a Rh model catalyst sample. As such, elevated pressure reactivity measurements on Rh/SiO₂ samples, which are calibrated by Rh coverage, can be related to an estimate of average particle size (d_p) based on the STM measurements.
- (3) The tandem use of model catalyst surfaces and well-defined single crystal surfaces under identical reaction conditions can provide useful insights into behavior of model catalyst surfaces.

Acknowledgments

We gratefully acknowledge support of this work by the Department of Energy, Office of Basic Energy Sciences, Division of Chemical Sciences, Geosciences, and Biosciences (DE-FG02-95ER-14511), and the Robert A Welch Foundation.

References

- [1] Valden M, Lai X and Goodman D W 1998 *Science* **281** 1647
- [2] Goodman D W 1982 *Surf. Sci.* **123** L679–85
- [3] Baumer M and Freund H-J 1999 *Prog. Surf. Sci.* **61** 127
- [4] Goodman D W 2003 *J. Catal.* **216** 213–22
- [5] Rupprechter G 2007 *Catal. Today* **126** 3
- [6] Poppa H 1993 *Catal. Rev.* **35** 359
- [7] Henry C R 1998 *Surf. Sci. Rep.* **31** 231
- [8] Grass M E, Zhang Y, Butcher D R, Park J Y, Li Y, Bluhm H, Bratlie K M, Zhang T and Somorjai G A 2008 *Angew. Chem. Int. Edn* **47** 8893
- [9] Frank M, Kühnemuth R, Bäumer M and Freund H-J 2000 *Surf. Sci.* **454** 968
- [10] Frank M, Kühnemuth R, Bäumer M and Freund H-J 1999 *Surf. Sci.* **427** 288
- [11] Frank M, Andersson S, Libuda J, Stempel S, Sandell A, Brena B, Giertz A, Brühwiler P A, Bäumer M, Mårtensson N and Freund H-J 1997 *Chem. Phys. Lett.* **279** 92
- [12] Nehasil V, Stará I and Matolín V 1996 *Surf. Sci.* **352** 305
- [13] Matolín V, Elyakhloufi M H, Mašek K and Gillet E 1993 *Catal. Lett.* **21** 175
- [14] Matolín V, Mašek K, Elyakhloufi M H and Gillet E 1993 *J. Catal.* **143** 492
- [15] Labich S, Taglauer E and Knözinger H 2001 *Top. Catal.* **14** 153
- [16] Dudin P, Barinov A, Gregoratti L, Scaini D, He Y B, Over H and Kiskinova M 2008 *J. Phys. Chem. C* **112** 9040–4
- [17] Park J B, Ratliff J S, Ma S and Chen D A 2007 *J. Phys. Chem. C* **111** 2165
- [18] Penner S, Wang D, Jenewein B, Gabasch H, Klötzer B, Knop-Gericke A, Schlögl R and Hayek K 2006 *J. Chem. Phys.* **125** 094703
- [19] Berkó A and Solymosi F 1999 *J. Catal.* **183** 91
- [20] Óvári L and Kiss J 2006 *Appl. Surf. Sci.* **252** 8624
- [21] Nolte P, Stierle A, Jin-Phillipp N Y, Kasper N, Schulli T U and Dosch H 2008 *Science* **321** 1654
- [22] Rupprechter G, Hayek K and Hofmeister H 1998 *J. Catal.* **173** 409
- [23] Tao F, Grass M E, Zhang Y, Butcher D R, Renzas J R, Liu Z, Chung J Y, Mun B S, Salmeron M and Somorjai G A 2008 *Science* **322** 322
- [24] Szanyi J and Goodman D W 1993 *Rev. Sci. Instrum.* **64** 2350
- [25] McClure S M, Lundwall M, Yang F, Zhou Z and Goodman D W 2009 *J. Phys. Chem. C* **113** 9688–97
- [26] Chen M S, Santra A K and Goodman D W 2004 *Phys. Rev. B* **69** 155404
- [27] Xu X and Goodman D W 1992 *Appl. Phys. Lett.* **61** 774
- [28] Chen M S, Cai Y, Yan Z, Gath K K, Axnanda S and Goodman D W 2007 *Surf. Sci.* **601** 5326
- [29] Blyholder G 1964 *J. Phys. Chem.* **68** 2772
- [30] Linke R, Curulla D, Hopstaken M J P and Niemantsverdriet J W 2001 *J. Chem. Phys.* **115** 8209
- [31] Fiorin V, McCoustra M R S and Chesters M A 2003 *J. Phys. Chem. B* **107** 7058
- [32] Gao F, Cai Y, Gath K K, Wang Y, Chen M S, Guo Q L and Goodman D W 2009 *J. Phys. Chem. C* **113** 182–92
- [33] Nakamura I, Kobayashi Y, Hamada H and Fujitani T 2006 *Surf. Sci.* **600** 3235
- [34] Evans J, Hayden B, Mosselmans F and Murray A 1992 *Surf. Sci. Lett.* **279** L159
- [35] Trautmann S and Baerns M 1994 *J. Catal.* **150** 335
- [36] Cavanagh R R and Yates J T Jr 1981 *J. Chem. Phys.* **74** 4150
- [37] Anderson J A 1991 *J. Chem. Soc. Faraday Trans.* **87** 3907
- [38] Shanks B H and Bailey J E 1988 *J. Catal.* **110** 197
- [39] Kiss J T and Gonzalez R D 1984 *J. Phys. Chem.* **88** 898
- [40] Goodman D W and Peden C H F 1986 *J. Phys. Chem.* **90** 4839
- [41] Peden C H F, Goodman D W, Blair D S, Berlowitz P J, Fisher G B and Oh S H 1988 *J. Phys. Chem.* **92** 1563
- [42] Oh S H, Fisher G B, Carpenter J E and Goodman D W 1986 *J. Catal.* **100** 360
- [43] Kiss J T and Gonzalez R D 1984 *J. Phys. Chem.* **88** 898
- [44] Cant N W, Hicks P C and Lennon B S 1978 *J. Catal.* **54** 372
- [45] Oh S H and Eickel C C 1991 *J. Catal.* **128** 526
- [46] Engel T and Ertl G 1979 *Adv. Catal.* **28** 1
- [47] Hopstaken M J P and Niemantsverdriet J W 2000 *J. Chem. Phys.* **113** 5457
- [48] Bowker M, Guo Q, Li Y and Joyner R W 1993 *Catal. Lett.* **18** 119
- [49] Berlowitz P J, Peden C H F and Goodman D W 1988 *J. Phys. Chem.* **92** 5213
- [50] Belton D N and Schmeig S J 1988 *Surf. Sci.* **202** 238
- [51] Zhu Y and Schmidt L D 1983 *Surf. Sci.* **129** 107